



# CHORUS

This is the accepted manuscript made available via CHORUS. The article has been published as:

## Electrohydrodynamic migration and dispersion of polyelectrolytes during simultaneous shear flow and electrophoresis

Dmitry I. Kopelevich and Jason E. Butler

Phys. Rev. Fluids **6**, 094203 — Published 22 September 2021

DOI: [10.1103/PhysRevFluids.6.094203](https://doi.org/10.1103/PhysRevFluids.6.094203)

# Electrohydrodynamic migration and dispersion of polyelectrolytes during simultaneous shear flow and electrophoresis

Dmitry I. Kopelevich\* and Jason E. Butler†

*Department of Chemical Engineering,  
University of Florida, Gainesville, FL 32611-6005, USA*

(Dated: August 30, 2021)

## Abstract

We develop a mean-field model for an elastic dumbbell that predicts an enhanced concentration of flexible polyelectrolytes in the center of a microfluidic channel due to simultaneous application of axial flow and electric fields. Consistent with previous works, the model indicates that local shear flow stretches and orients a polyelectrolyte molecule so that electrohydrodynamic interactions within the molecule drive its migration towards the center of the channel. Unlike previous works, dispersion due to fluctuations of electrohydrodynamic velocity induced by thermal fluctuations of the molecular configuration is explicitly included in the mean-field model. This electrohydrodynamic dispersion is comparable with or exceeds diffusivity due to Brownian forces for electric field strengths commonly used in microfluidic devices. The developed models are in quantitative agreement with Brownian dynamics simulations and in qualitative agreement with experiments. In particular, competition between the electrohydrodynamic migration and dispersion is shown to cause a non-monotonic dependence of the polyelectrolyte concentration in the channel center on the magnitude of the electric field.

## I. INTRODUCTION

Electric fields are commonly utilized to manipulate macromolecular transport within microfluidic devices for analysis and processing, and researchers continue to discover new and varied ways to use electric fields within microfluidic devices. For the particular case of polyelectrolyte molecules, such as DNA, simultaneous application of an axial electric field and pressure-driven flow can cause a transverse migration and subsequent concentration of polyelectrolytes at either the wall or the centerline of the channel [1–3]. This migration phenomenon has been used to trap and separate DNA within a microfluidic device of simple design [4–6].

The transverse migration is caused by electrohydrodynamic interactions between different portions of a polyelectrolyte molecule, i.e. interactions due to disturbances in the fluid flow caused by an external electric field acting on the charged polymer and its surrounding counterions [7–12]. These interactions are of importance to the dynamics of a polyelectrolyte if

---

\* dkopelevich@che.ufl.edu

† butler@che.ufl.edu

the double layer is large compared to the diameter of the polymer backbone and the molecule is distorted from its equilibrium ~~(roughly spherical)~~ isotropic configuration. In the case of migration in a pressure-driven flow, a molecule not at the center of the channel is stretched and reoriented by a local shear. Then, the electric field and resulting electrohydrodynamic interactions induce additional components of motion, including one transverse to the flow and field direction.

When a flexible polyelectrolyte leads a pressure-driven flow upon application of an axial electric field, the transverse motion is towards the center of the channel, as illustrated in Fig. 1. The electrohydrodynamic velocity is proportional to the magnitude of the electric field, which suggests that increasing strength of the electric field should increase concentration of polyelectrolytes in the center of the channel. However, experiments [3] and simulations [9] show that this trend holds only for weak electric fields; for sufficiently strong fields, the concentration at the channel center decreases as the field strength increases. In other words, there is an optimal field strength  $E^*$  corresponding to the smallest width  $\sigma$  of the concentration profile at the channel center.

The kinetic model of Butler et al. [8] predicted a monotonic decrease of the concentration profile width with increasing electric field for a dumbbell in a pressure-driven flow, in contrast with later findings [3, 9]. More recently, Setaro and Underhill [13] developed an improved kinetic model that accounts for fluctuations of the end-to-end vector of the dumbbell and predicts a non-monotonic dependence of the centerline concentration on the electric field. They attributed this phenomenon to feedback between the polymer flux and conformation.

To further clarify the physical origin of the minimum value for  $\sigma$ , Kopelevich et al. [14] suggested an empirical model that includes dispersion due to the electric field. This electrohydrodynamic dispersion arises from the instantaneous electrohydrodynamic velocity corresponding to each configuration of the fluctuating polyelectrolyte molecule. The average of these instantaneous velocities corresponds to the migration velocity driving the polymer towards the center of the channel, while the velocity fluctuations contribute to the effective polymer diffusivity. The electrohydrodynamic dispersion increases with the strength of the electric field faster than the migration velocity. Since the profile width  $\sigma$  is determined by competition between the migration towards the center of the channel and diffusive flux away from the center,  $\sigma$  increases with increasing field strength for sufficiently strong electric fields. This empirical model was confirmed by Brownian dynamics simulations for a multi-

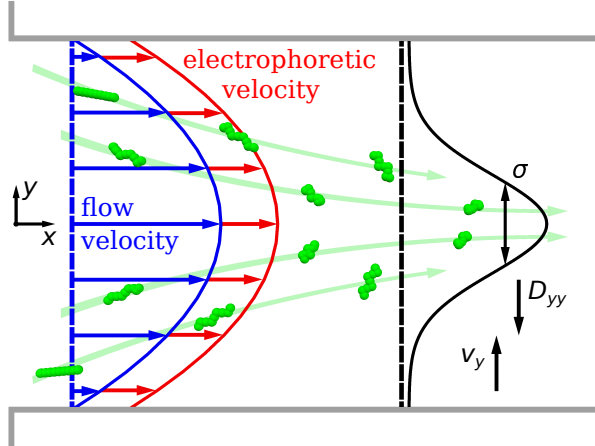


Figure 1: **Trapping Focusing** of DNA molecules in the center of a microfluidic channel by simultaneous application of a pressure-driven flow (blue) and an anti-parallel electric field. The electric field causes the negatively charged DNA molecules to lead the flow (red) and migrate towards the center of the channel (green arrows). The width  $\sigma$  of the developed concentration profile (black) is determined by competition between the net migration  $V_y$  towards the center and diffusion  $D_{yy}$  away from the center. The diffusivity  $D_{yy}$  contains contributions from Brownian diffusion and electrohydrodynamic dispersion.

bead polymer model [14].

In this work, we develop explicit mean-field relationships between the dispersion and dynamics of the internal degrees of freedom of a dumbbell in shearing and pressure-driven flows. The mean-field model developed for a shearing flow directly connects the electrohydrodynamic dispersion with the autocorrelation function of instantaneous electrohydrodynamic velocity which, in turn, is determined by the end-to-end vector of the dumbbell. For the pressure-driven flow, the mean-field model is a convection-diffusion equation with the diffusion term containing contributions of both the Brownian diffusivity and the electrohydrodynamic dispersion. We derive this model by performing an adiabatic elimination of the internal degrees of freedom from the Fokker-Planck equation for the harmonic approximation of a dumbbell with short-range electrohydrodynamic interactions. The resulting equation is consistent with the kinetic theory of Setaro and Underhill [13], but our new derivation clearly demonstrates the contribution of electrohydrodynamic dispersion to the polymer flux.

In Section II, we present Langevin equations for the center of mass and the internal degrees of freedom of the dumbbell. In Section III, we consider the dumbbell in a shearing flow and develop and validate mean-field relationships between transport properties of the dumbbell and statistics of its internal degrees of freedom. In Section IV, we discuss the mean-field model for the dumbbells in a pressure-driven flow, demonstrate the generic nature of the dispersion mechanism leading to the non-monotonic dependence of the concentration profile width on the electric field strength, and discuss the effect of the time-scale separation (or lack thereof) on parameters of the mean-field model. Conclusions are presented in Section V.

## II. MODEL

The current work models  $\lambda$ -DNA molecules that were used in the experiments of Arca et al. [3]. These molecules have a contour length of approximately  $21 \mu\text{m}$ , which is substantially larger than their Kuhn length of  $106 \text{ nm}$  [15]. Therefore, a  $\lambda$ -DNA molecule is flexible and each bead of its dumbbell model represents a large number of Kuhn steps so that the beads can be approximated as spheres.

The ~~polyelectrolyte molecule is modeled as a~~ dumbbell is suspended in an ambient flow field  $\mathbf{U}^\infty(\mathbf{R})$  and a uniform electric field  $\mathbf{E}$ . The dynamics of each bead is described by the following Langevin equation:

$$\frac{d\mathbf{R}_i}{dt} = \mathbf{U}^\infty(\mathbf{R}_i) + \frac{1}{\zeta}(\mathbf{F}_i^C + \mathbf{F}_i^B) + \mu_0^E \mathbf{E} + \mathbf{U}_i^E, \quad i = 1, 2. \quad (1)$$

Here,  $\mathbf{R}_i$  are coordinates of the dumbbell beads,  $\mathbf{F}_i^C$  and  $\mathbf{F}_i^B$  are the conservative and Brownian forces acting on the  $i$ -th bead ( $i = 1, 2$ ),  $\zeta = 6\pi\eta a$  is the friction coefficient of a spherical bead of radius  $a$  in a fluid with viscosity  $\eta$ ,  $\mu_0^E$  is the electrophoretic mobility, and  $\mathbf{U}_i^E$  is the electrohydrodynamic velocity of the  $i$ -th bead. The Brownian force satisfies the fluctuation-dissipation theorem [16],

$$\langle \mathbf{F}_i^B(t) \rangle = 0, \quad (2)$$

$$\langle \mathbf{F}_i^B(t) \mathbf{F}_j^B(t + \tau) \rangle = 2k_B T \zeta \mathbf{I} \delta_{ij} \delta(\tau), \quad i, j = 1, 2. \quad (3)$$

where  $k_B$  is the Boltzmann constant,  $T$  is the temperature,  $\mathbf{I}$  is the  $3 \times 3$  identity matrix,  $\delta_{ij}$  is the Kronecker delta, and  $\delta(\tau)$  is the Dirac delta-function.

For simplicity, here we neglect hydrodynamic interactions due to velocity disturbances caused by Brownian and conservative forces. Effects of these hydrodynamic interactions

are explored in Section S1 of Supplemental Material [17], where it is shown that the main conclusions of this work remain valid if these interactions are taken into account.

The polymer is assumed to be sufficiently far from the channel walls so that the polymer-wall interactions are negligible. In this case, the only contribution to the conservative forces  $\mathbf{F}_i^C$  is the bead-bead interactions and the potential  $\Phi$  for these forces depends only on the distance between the beads,

$$\mathbf{F}_2^C = -\mathbf{F}_1^C = -\frac{\partial\Phi(q)}{\partial\mathbf{q}} \equiv \mathbf{F}^C(\mathbf{q}), \quad (4)$$

where  $\mathbf{q} = \mathbf{R}_2 - \mathbf{R}_1$  is the end-to-end vector. The dumbbell beads are connected by a freely jointed chain of  $N_K$  Kuhn steps of length  $l_K$  each, with the tension approximated by the finitely extensible nonlinear elastic (FENE) force [18],

$$\mathbf{F}^C(\mathbf{q}) = -\frac{\kappa\mathbf{q}}{1 - (q/q_0)^2}, \quad (5)$$

where  $q_0 = N_K l_K$  is the maximum extension of the spring and  $\kappa = 3k_B T / l_K q_0$  is the spring constant. For  $\lambda$ -DNA molecules considered in the current work,  $N_K = 200$  and  $l_K = 106$  nm [15].

We use the short-range model for electrohydrodynamic interactions [10–12]. Within this model, the electrohydrodynamic mobility of a dumbbell is approximated by an average of electrohydrodynamic mobilities of Kuhn steps of the spring connecting the dumbbell beads; electrohydrodynamic interactions between the Kuhn steps and between the beads are neglected. Both dumbbell beads have the same electrohydrodynamic velocity, which can be written as

$$\mathbf{U}_i^E(\mathbf{q}) = \mathcal{E}\hat{\mathbf{U}}^E(\mathbf{q}), \quad i = 1, 2. \quad (6)$$

Here,

$$\mathcal{E} = \frac{1 - \alpha_\mu}{1 + 2\alpha_\mu} \frac{2\mu_0^E E}{q_0^2} \quad (7)$$

quantifies the strength  $E$  of the electric field and  $\alpha_\mu = \mu_\perp^E / \mu_\parallel^E$  is the ratio of the electrohydrodynamic mobilities  $\mu_\perp^E$  and  $\mu_\parallel^E$  of a Kuhn step (modeled as a rod) in the directions perpendicular and parallel to the rod axis. The normalized electrohydrodynamic velocity is

$$\hat{\mathbf{U}}^E(\mathbf{q}) = \frac{(3\mathbf{q}\mathbf{q} - q^2\mathbf{I}) \cdot \hat{\mathbf{E}}}{3 - (q/q_0)^2}, \quad (8)$$

where  $\hat{\mathbf{E}} = \mathbf{E}/E$  is the direction of the electric field.

In what follows, we non-dimensionalize the variables using the characteristic length  $l_c = \sqrt{k_B T / \kappa}$ , the characteristic time  $t_c = \zeta / \kappa$ , the characteristic energy  $k_B T$ , and the elementary charge  $e$ . The dimensionless values of  $\kappa$  and  $\zeta$  are 1.

Subtracting and adding the Langevin equations (1) for beads 1 and 2 and using Eqs. (4) and (6), we obtain the following equations for the end-to-end vector  $\mathbf{q}$  and the center of mass  $\mathbf{R}_c = (\mathbf{R}_1 + \mathbf{R}_2)/2$  of the dumbbell:

$$\frac{d\mathbf{q}}{dt} = (\mathbf{q} \cdot \nabla) \mathbf{U}^\infty(\mathbf{R}_c) + 2\mathbf{F}^C(\mathbf{q}) + \mathbf{F}_q^B(t), \quad (9)$$

$$\frac{d\mathbf{R}_c}{dt} = \mathbf{U}^\infty(\mathbf{R}_c) + \mu_0^E \mathbf{E} + \mathcal{E} \hat{\mathbf{U}}^E(\mathbf{q}) + \mathbf{F}_c^B(t). \quad (10)$$

In writing Eqs. (9) and (10), we kept only the leading order terms of the expansion of  $\mathbf{U}^\infty(\mathbf{R})$  around the dumbbell center of mass. The stochastic forces acting on  $\mathbf{q}$  and  $\mathbf{R}_c$  are

$$\mathbf{F}_q^B = \mathbf{F}_2^B - \mathbf{F}_1^B \quad \text{and} \quad \mathbf{F}_c^B = \frac{1}{2} (\mathbf{F}_1^B + \mathbf{F}_2^B), \quad (11)$$

respectively. These forces have zero mean and their autocorrelation functions are

$$\langle \mathbf{F}_q^B(t) \mathbf{F}_q^B(t + \tau) \rangle = 4\mathbf{I} \delta(\tau), \quad (12)$$

$$\langle \mathbf{F}_c^B(t) \mathbf{F}_c^B(t + \tau) \rangle = \mathbf{I} \delta(\tau), \quad (13)$$

$$\langle \mathbf{F}_q^B(t) \mathbf{F}_c^B(t + \tau) \rangle = 0, \quad (14)$$

where the last equality indicates that  $\mathbf{F}_q^B(t)$  and  $\mathbf{F}_c^B(t)$  are independent of each other.

Equation (10) shows that motion of the polymer center of mass  $\mathbf{R}_c$  is affected by dynamics of the internal degrees of freedom  $\mathbf{q}(t)$ . Random fluctuations of  $\mathbf{q}$  lead to fluctuations of the electrohydrodynamic velocity  $\mathcal{E} \hat{\mathbf{U}}^E(\mathbf{q})$ , which give rise to electrohydrodynamic dispersion.

### III. ELECTROHYDRODYNAMIC DISPERSION IN A SHEARING FLOW

In this section we consider the dumbbell in a shearing flow  $\mathbf{U}^\infty(\mathbf{R}) = \boldsymbol{\gamma} \cdot (\mathbf{R} - \mathbf{R}_c)$ , where  $\boldsymbol{\gamma}$  is a position-independent rate-of-strain tensor. We demonstrate that fluctuations of the end-to-end vector  $\mathbf{q}$  of the dumbbell yield electrohydrodynamic dispersion and obtain an explicit expression for the dispersion contribution to the overall diffusivity of the dumbbell. To obtain the relationship between statistics of the vector  $\mathbf{q}$  and the electrohydrodynamic

dispersion, the average and fluctuating components of the center of mass position and the electrohydrodynamic velocity are separated,

$$\mathbf{R}_c(t) = \langle \mathbf{R}_c \rangle(t) + \mathbf{r}_c(t), \quad (15)$$

$$\hat{\mathbf{U}}^E(\mathbf{q}(t)) = \langle \hat{\mathbf{U}}^E \rangle + \hat{\mathbf{u}}^E(\mathbf{q}(t)), \quad (16)$$

where  $\mathbf{r}_c(t)$  and  $\hat{\mathbf{u}}^E(\mathbf{q}(t))$  represent fluctuations of  $\mathbf{R}_c(t)$  and  $\hat{\mathbf{U}}^E$  around their mean values. Eq. (9) indicates that the end-to-end vector is independent of the translational motion of the dumbbell in a shearing flow. Therefore,  $\langle \hat{\mathbf{U}}^E \rangle$  is independent of time and can be obtained by averaging over the steady-state solution  $\mathbf{q}(t)$  of Eq. (9). It then follows from Eq. (10) that the mean and the fluctuating components of the dumbbell center of mass obey the following equations:

$$\frac{d\langle \mathbf{R}_c \rangle}{dt} = \mu_0^E \mathbf{E} + \mathcal{E} \langle \hat{\mathbf{U}}^E \rangle, \quad (17)$$

$$\frac{d\mathbf{r}_c}{dt} = \mathcal{E} \hat{\mathbf{u}}^E(\mathbf{q}(t)) + \mathbf{F}_c^B(t). \quad (18)$$

We note that  $\mathbf{U}^\infty(\mathbf{R}_c) = 0$  for the shearing flow. The right-hand side of Eq. (18) contains two fluctuating terms. One of these terms,  $\mathbf{F}_c^B(t)$ , corresponds to the usual Brownian force. The other term,  $\mathcal{E} \hat{\mathbf{u}}^E(\mathbf{q}(t))$ , represents instantaneous deviations of the electrohydrodynamic velocity from its mean value  $\mathcal{E} \langle \hat{\mathbf{U}}^E \rangle$ . These deviations are caused by fluctuations of the end-to-end vector  $\mathbf{q}(t)$  and give rise to the electrohydrodynamic dispersion.

Integrating Eq. (18), we obtain

$$\mathbf{r}_c(t) - \mathbf{r}_c(0) = \int_0^t [\mathcal{E} \hat{\mathbf{u}}^E(\mathbf{q}(s)) + \mathbf{F}_c^B(s)] ds. \quad (19)$$

Hence, the diffusion tensor of the dumbbell center of mass is

$$\begin{aligned} \mathbf{D} &= \lim_{t \rightarrow \infty} \frac{1}{2t} \langle [\mathbf{r}_c(t) - \mathbf{r}_c(0)][\mathbf{r}_c(t) - \mathbf{r}_c(0)] \rangle \\ &= \lim_{t \rightarrow \infty} \frac{1}{2t} \int_0^t \int_0^t \langle [\mathcal{E} \hat{\mathbf{u}}^E(\mathbf{q}(s)) + \mathbf{F}_c^B(s)][\mathcal{E} \hat{\mathbf{u}}^E(\mathbf{q}(s')) + \mathbf{F}_c^B(s')] \rangle ds ds' \\ &= \mathbf{D}^E + \mathbf{D}^B, \end{aligned} \quad (20)$$

where

$$\mathbf{D}^E = \lim_{t \rightarrow \infty} \frac{\mathcal{E}^2}{2t} \int_0^t \int_0^t \langle \hat{\mathbf{u}}^E(\mathbf{q}(s)) \hat{\mathbf{u}}^E(\mathbf{q}(s')) \rangle ds ds' \quad (21)$$

is the electrohydrodynamic dispersion and

$$\mathbf{D}^{\mathbf{B}} = \lim_{t \rightarrow \infty} \frac{1}{2t} \int_0^t \int_0^t \langle \mathbf{F}_c^{\mathbf{B}}(s) \mathbf{F}_c^{\mathbf{B}}(s') \rangle ds ds' = \frac{1}{2} \mathbf{I} \quad (22)$$

is the diffusivity in the absence of the electric field, i.e. the usual Brownian diffusivity. In writing the last equality in Eq. (20), we took into account that  $\hat{\mathbf{u}}^E(\mathbf{q}(t))$  and  $\mathbf{F}_c^{\mathbf{B}}(t)$  are uncorrelated, since the random force  $\mathbf{F}_q^{\mathbf{B}}(t)$  acting on the end-to-end vector  $\mathbf{q}(t)$  is not correlated with the Brownian force  $\mathbf{F}_c^{\mathbf{B}}(t)$  acting on the center of mass (see Eq. (14)).

Since  $\hat{\mathbf{u}}^E$  is independent of the field strength, Eqs. (20) and (21) demonstrate that the mean square displacement is increased by a factor proportional to  $\mathcal{E}^2$  due to fluctuations in the electrohydrodynamic interactions. To obtain the electrohydrodynamic dispersion, we rewrite Eq. (21) as follows:

$$\mathbf{D}^{\mathbf{E}} = \lim_{t \rightarrow \infty} \frac{\mathcal{E}^2}{2t} \int_0^t \int_{-s}^{t-s} \mathbf{C}^{\mathbf{E}}(\tau) d\tau ds = \frac{\mathcal{E}^2}{2} \int_{-\infty}^{\infty} \mathbf{C}^{\mathbf{E}}(\tau) d\tau. \quad (23)$$

Here,

$$\mathbf{C}^{\mathbf{E}}(\tau) = \langle \hat{\mathbf{u}}^E(\mathbf{q}(s)) \hat{\mathbf{u}}^E(\mathbf{q}(s + \tau)) \rangle \quad (24)$$

is the autocorrelation function of  $\hat{\mathbf{u}}^E(\mathbf{q}(t))$ . The last equality in Eq. (23) was obtained by replacing the limits of integration in the inner integral by  $\pm\infty$ . This approximation is justified by the time-scale separation between fluctuations of the end-to-end vector and diffusive motion, so that  $\mathbf{C}^{\mathbf{E}}(\tau) \approx 0$  for  $\tau$  on the diffusive time-scale.

Dispersion in shearing flows can thus be obtained by solving the Langevin equation (9) for the end-to-end vector and then computing the integral of the autocorrelation function of the instantaneous electrohydrodynamic velocity using the mean-field equations (23) and (24). In the remainder of this section, we obtain transport properties of the dumbbell in a simple shear flow

$$\mathbf{U}^\infty(\mathbf{R}) = [\gamma(y - y_c), 0, 0]^T, \quad (25)$$

where  $\gamma$  is the shear rate and  $y_c$  is the  $y$ -coordinate of the dumbbell center of mass. The electric field is assumed to be parallel to the flow. At sufficiently small shear rates, the transport properties can be obtained analytically. In this case, the harmonic approximation to the FENE spring potential (5) is used,

$$\mathbf{F}^C(\mathbf{q}) = -\mathbf{q}. \quad (26)$$

In addition, ~~the harmonic approximation to~~ the transverse component of the normalized electrohydrodynamic velocity (8) is ~~approximated by~~

$$\hat{U}_y^E = q_x q_y. \quad (27)$$

For brevity, we refer to the model with the harmonic spring potential Eq. (26) and the leading order approximation Eq. (27) to the electrohydrodynamic interactions as the “harmonic dumbbell” and the model with the FENE spring potential Eq. (5) and the electrohydrodynamic interactions given by Eq. (8) as the “FENE dumbbell”.

Note that the harmonic dumbbell model is linear only for the internal degrees of freedom  $\mathbf{q}$ , since the electrohydrodynamic interactions influencing motion of the dumbbell center of mass are nonlinear even in the leading-order approximation Eq. (27). It is shown in Appendix A that, ~~in this case,~~ for the harmonic dumbbell, the mean electrohydrodynamic velocity and dispersion in the transverse direction are

$$\langle U_y^E \rangle(\gamma, \mathcal{E}) = \frac{\mathcal{E}\gamma}{4} \quad \text{and} \quad D_{yy}^E(\gamma, \mathcal{E}) = \frac{\mathcal{E}^2}{4} \left( 1 + \frac{5\gamma^2}{16} \right), \quad (28)$$

respectively. Figure 2 shows the analytical mean-field result (28) as a function of the Weissenberg number  $\text{Wi} = \tau_r \gamma$ , where  $\tau_r = 1/4$  is the relaxation time of the end-to-end distance of the dumbbell at equilibrium. We plot the normalized transverse velocity  $\langle \hat{U}_y^E \rangle = \langle U_y^E \rangle / \mathcal{E}$  and dispersion  $\hat{D}_{yy}^E = D_{yy}^E / \mathcal{E}^2$ , since these quantities are independent of the magnitude  $\mathcal{E}$  of the electric field. Additionally, Fig. 2 compares the analytical result for the harmonic dumbbell with simulation results for both harmonic and FENE dumbbells. ~~In the FENE dumbbell, the electrohydrodynamic velocity is modeled by Eq. (8).~~ Results of two types of simulations are shown in Fig. 2: semi-analytical mean-field calculations and direct Brownian dynamics simulations.

In the semi-analytical mean-field calculations, the Langevin equation (9) for the end-to-end vector was solved numerically. For each set of the system parameters, at least 200 simulations of duration 5000 were performed. The mean transverse velocity  $\langle \hat{U}_y^E \rangle$  was then obtained by averaging the instantaneous values of the electrohydrodynamic velocity  $\hat{U}_y^E(\mathbf{q})$ , with vector  $\mathbf{q}(t)$  obtained from the numerical solution. The transverse dispersion  $\hat{D}_{yy}^E$  was obtained by integrating the autocorrelation function of the instantaneous velocity, see Eqs. (23) and (24).

For the Brownian dynamics simulations, the Langevin equations (1) for the individual beads were integrated numerically. At least  $10^4$  simulations of duration 5000 each were

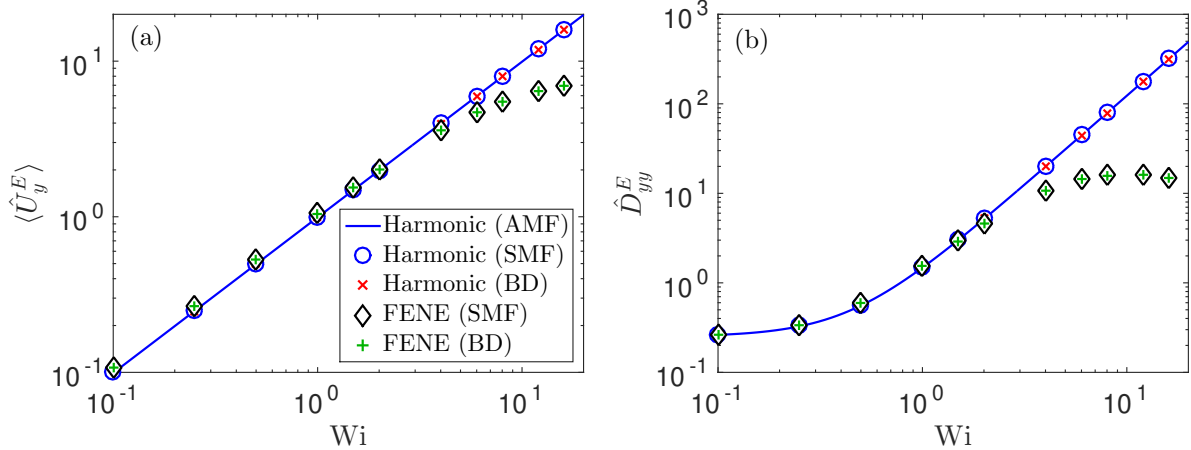


Figure 2: (a) Normalized mean electrohydrodynamic velocity  $\langle \hat{U}_y^E \rangle = \langle U_y^E \rangle / \mathcal{E}$  and (b) normalized electrohydrodynamic dispersion  $\hat{D}_{yy}^E = D_{yy}^E / \mathcal{E}^2$  in the transverse direction in a simple shear flow. Transport properties of the harmonic and FENE dumbbell models are shown. Predictions of the analytical mean-field (AMF) model (28) for the harmonic dumbbell are shown by lines; predictions of the semi-analytical mean-field (SMF) model are shown by open symbols, and results of the Brownian dynamics (BD) simulations are shown by crosses.

performed for each set of parameters. The mean dumbbell velocity and diffusivity  $\mathbf{D}$  were then obtained by fitting the mean displacement and the mean-squared displacement of the dumbbell center of mass to a straight line [14]. The normalized electrohydrodynamic dispersion was computed as  $\hat{\mathbf{D}}^E = (\mathbf{D} - \mathbf{D}^B) / \mathcal{E}^2$ , where the Brownian diffusivity  $\mathbf{D}^B$  was obtained from simulations with no electric field.

As evident from Fig. 2, the mean-field model is in excellent agreement with the Brownian dynamics simulations. We also verified that  $\mathbf{D}^B$  obtained from the Brownian dynamics simulations is  $\mathbf{I}/2$ , in agreement with Eq. (22), and that  $(\mathbf{D} - \mathbf{D}^B)$  scales as  $\mathcal{E}^2$ , in agreement with Eqs. (20) and (21).

Fig. 2 shows that the short-range electrohydrodynamic model predicts a monotonic growth of the mean transverse velocity and dispersion with increasing shear rate. Increasing the shear rate leads to changes of the dumbbell configuration, including its reorientation and stretching. In particular, stretching of the dumbbell spring results in increasing electrohydrodynamic velocity predicted by the short-range model Eq. (8). The harmonic dumbbell

approximation is in good agreement with the full anharmonic model for  $Wi \leq 2$ . For  $Wi > 2$ , the harmonic model predicts larger values of electrohydrodynamic velocity and dispersion, due to a larger stretching of the harmonic spring in comparison with the FENE spring at high shear rates, [see Section S2 of Supplemental Material \[17\]](#).

## IV. EFFECT OF DISPERSION ON CONCENTRATION PROFILES IN PRESSURE-DRIVEN FLOWS

### A. General considerations

As illustrated in Fig. 1, the distribution of polyelectrolytes in a pressure-driven flow is determined by a balance between the flux towards the channel center due to the electrohydrodynamic migration  $V_y = \mathcal{E}\langle\hat{U}_y^E\rangle$  and the flux away from the channel center due to diffusive motion of the polymers. For a weak electric field, the diffusivity  $D_{yy}$  is dominated by Brownian motion and is essentially independent of the field strength, whereas the driving force towards the center of the channel is proportional to  $\mathcal{E}$ . Therefore, at weak fields, the concentration profile width  $\sigma$  decreases as the field strength increases. However, the electrohydrodynamic dispersion  $\mathbf{D}^E$  scales quadratically with the electric field as shown in the previous section. When the field is sufficiently strong, the diffusive flux is dominated by the electrohydrodynamic dispersion, which increases faster with  $\mathcal{E}$  than the migration velocity  $\mathcal{E}\langle\hat{U}_y^E\rangle$  does. Therefore, increasing the field strength beyond the optimal value  $\mathcal{E}^*$  leads to wider concentration profiles.

Here we develop a mean-field model for polymer density  $n$  in a pressure-driven flow that accounts for the dispersion and demonstrates a minimum for the profile width  $\sigma$ . The pressure-driven flow is ~~centered at  $y = 0$  and the channel walls are between two infinite,~~ **planar walls** located at  $y = \pm H/2$ . The electric field and the fluid flow are parallel to the  $x$ -axis and the shear rate is

$$\gamma(y) = \frac{dU_x^\infty(y)}{dy} = -\frac{4\bar{\gamma}y}{H}, \quad (29)$$

where  $\bar{\gamma}$  is the mean shear rate.

The polymer density  $n$  in a fully-developed steady-state flow is assumed to satisfy the

convection-diffusion equation,

$$\frac{d}{dy_c} \left[ D_{yy}^{\text{eff}}(y_c, \mathcal{E}) \frac{dn}{dy_c} - V_y(y_c, \mathcal{E})n \right] = 0. \quad (30)$$

Here,  $V_y$  and  $D_{yy}^{\text{eff}}$  are the mean migration velocity and the effective diffusivity in the transverse direction, where  $D_{yy}^{\text{eff}}$  contains contributions of both Brownian diffusivity and the electrohydrodynamic dispersion. If the time-scale of the translational motion of the polymer is much slower than that of its internal dynamics, the polymer configuration adjusts its dynamics to the local shear as the polymer moves across streamlines of a flow. In this case, the transport properties of the polymer are fully determined by the local shear, i.e.

$$V_y(y_c, \mathcal{E}) = \langle U_y^E \rangle(\gamma(y_c), \mathcal{E}) \quad \text{and} \quad D_{yy}^{\text{eff}}(y_c, \mathcal{E}) = D_{yy}^{\text{ss}}(\gamma(y_c), \mathcal{E}), \quad (31)$$

where

$$\langle U_y^E \rangle(\gamma, \mathcal{E}) = \mathcal{E} \langle \hat{U}_y^E \rangle(\gamma) \quad \text{and} \quad D_{yy}^{\text{ss}}(\gamma, \mathcal{E}) = D_{yy}^B(\gamma) + \mathcal{E}^2 \hat{D}_{yy}^E(\gamma) \quad (32)$$

are the migration velocity and diffusivity in the simple shear flow at shear rate  $\gamma$  and the electric field strength  $\mathcal{E}$ . The normalized migration velocity  $\langle \hat{U}_y^E \rangle(\gamma)$ , the Brownian diffusivity  $D_{yy}^B(\gamma)$ , and the normalized electrohydrodynamic dispersion  $\hat{D}_{yy}^E(\gamma) = D_{yy}^E(\gamma, \mathcal{E})/\mathcal{E}^2$  are independent of  $\mathcal{E}$ .

It follows from Eq. (30) that

$$n(y_c) \propto \exp \int_0^{y_c} \frac{V_y(y', \mathcal{E})}{D_{yy}^{\text{eff}}(y', \mathcal{E})} dy'. \quad (33)$$

It was shown by Kopelevich et al. [14] that Eq. (33) yields a Gaussian distribution,  $n \propto \exp(-y_c^2/2\sigma^2)$ , if  $\langle U_y^E \rangle \propto \gamma$  and dependence of  $D_{yy}^{\text{ss}}$  on  $\gamma$  is weak in the region of high concentration of polymers. In this case, the standard deviation of  $n$  is determined by the ratio of the velocity and the diffusivity,  $\sigma \propto (D_{yy}^{\text{eff}}/V_y)^{1/2}$ . This ratio, according to Eqs. (31) and (32), is given by

$$\frac{D_{yy}^{\text{eff}}}{V_y} = \frac{1}{\langle \hat{U}_y^E \rangle} \left( \frac{1}{\mathcal{E}} D_{yy}^B + \mathcal{E} \hat{D}_{yy}^E \right). \quad (34)$$

The first and second terms in Eq. (34) are monotonically decreasing and increasing functions of  $\mathcal{E}$ , respectively. Therefore, the ratio  $D_{yy}^{\text{eff}}/V_y$  and the profile width  $\sigma$  exhibit a minimum at some optimal electric field strength  $\mathcal{E} = \mathcal{E}^*$ .

## B. Mean-field model for the harmonic dumbbell approximation

The empirical mean-field model (30) was confirmed by Brownian dynamics simulations for a multi-bead polymer [14]. We demonstrate in this section that a similar mean-field model can be obtained using a more rigorous approach. Specifically, we consider a Fokker-Planck equation that describes dynamics of all degrees of freedom of the harmonic dumbbell and perform an adiabatic elimination of the internal degrees of freedom.

In the **harmonic leading order** approximation (26), (27), the  $z$ -component of the end-to-end vector  $\mathbf{q}$  is decoupled from all other degrees of freedom of the dumbbell and, hence, is omitted from the analysis. Therefore, in the remainder of this section,  $\mathbf{q}$  refers to the vector containing only the  $x$ - and  $y$ - components of the end-to-end vector. In addition, only the transverse coordinate  $y_c$  of the center of mass needs to be considered, since we focus on the dumbbell distribution in a fully-developed flow. This allows simplification of the Langevin equations (9), (10) to

$$\frac{dq_i}{dt} = \delta_{ix}\gamma(y_c)q_y - 2q_i + F_{q,i}^B(t), \quad i = x, y, \quad (35)$$

$$\frac{dy_c}{dt} = \mathcal{E}q_xq_y + F_{c,y}^B(t). \quad (36)$$

The corresponding Fokker-Planck equation is

$$\frac{\partial P}{\partial t} = \left[ \frac{1}{2} \frac{\partial^2}{\partial y_c^2} + 2L_q + L_{yq} \right] P, \quad (37)$$

where  $P(\mathbf{q}, y_c, t)$  is the probability density,

$$L_q = \frac{\partial}{\partial \mathbf{q}} \cdot \left( \mathbf{q} + \frac{\partial}{\partial \mathbf{q}} \right) \quad (38)$$

is the operator describing fluctuations of the end-to-end vector in the absence of shear, and the operator

$$L_{yq} = -\gamma(y_c)q_y \frac{\partial}{\partial q_x} - \mathcal{E}q_xq_y \frac{\partial}{\partial y_c} \quad (39)$$

describes coupling between the polymer center of mass and the end-to-end vector. There are two diffusive terms in Eq. (37): the Brownian diffusion of the dumbbell center of mass represented by the first term on the right-hand-side of Eq. (37) and random fluctuations of the end-to-end vector  $\mathbf{q}$  represented by the operator  $L_q$ . The fluctuations of  $\mathbf{q}$  give rise to the electrohydrodynamic dispersion through coupling with the center of mass motion described by the operator  $L_{yq}$ .

Similarly to analogous problems using adiabatic elimination [19],  $\mathbf{q}$  is eliminated from Eq. (37) by expanding  $P(\mathbf{q}, y_c, t)$  in terms of eigenfunctions of the operator  $L_q$ . As shown below, the leading term of this expansion corresponds to the equilibrium distribution of the end-to-end vector and the coefficient for that term corresponds to the number density  $n(y_c, t)$  of the dumbbells. Other terms of the expansion describe deviations from equilibrium and correspond to various moments of the end-to-end vector. These moments quickly relax towards values determined by  $n(y_c, t)$ , whereas the dynamics of  $n$  is relatively slow. This allows reducing equation (37) for  $P(\mathbf{q}, y_c, t)$  to a mean-field equation for  $n(y_c, t)$ .

To proceed, it is convenient to transform  $L_q$  into a self-adjoint operator by first defining

$$P(\mathbf{q}, y_c, t) = C_0^2 e^{-q^2/4} \bar{P}(\mathbf{q}, y_c, t), \quad (40)$$

where  $C_0 = (2\pi)^{-1/4}$  is a constant that ensures consistent normalization of the probability density, as shown in Appendix C. Then

$$L_q P = C_0^2 e^{-q^2/4} \bar{L}_q \bar{P}, \quad (41)$$

where

$$\bar{L}_q = -(b_x^\dagger b_x + b_y^\dagger b_y) \quad (42)$$

is the transformed self-adjoint operator for the equilibrium end-to-end vector dynamics and

$$b_i = \frac{\partial}{\partial q_i} + \frac{q_i}{2} \quad \text{and} \quad b_i^\dagger = -\frac{\partial}{\partial q_i} + \frac{q_i}{2} \quad (i = x, y) \quad (43)$$

are the boson annihilation and creation operators, respectively [19]. The eigenvalues of operators  $b_i^\dagger b_i$  are non-negative integers and the zero eigenvalue corresponds to the equilibrium distribution of the end-to-end vector. Additional properties of these operators and their eigenfunctions are reviewed in Appendix C.

The coupling operator  $L_{yq}$  is then expressed in terms of the operators  $b_i$  and  $b_i^\dagger$ . Since

$$\frac{\partial P}{\partial q_i} = -C_0^2 e^{-q^2/4} (b_i^\dagger \bar{P}) \quad \text{and} \quad q_i = b_i + b_i^\dagger \quad (i = x, y), \quad (44)$$

we have

$$L_{yq} P = C_0^2 e^{-q^2/4} \bar{L}_{yq} \bar{P}, \quad (45)$$

where

$$\bar{L}_{yq} = \gamma(\eta)(b_y + b_y^\dagger)b_x^\dagger - \epsilon\mathcal{E}(b_x + b_x^\dagger)(b_y + b_y^\dagger)\frac{\partial}{\partial\eta} \quad (46)$$

is the transformed operator  $L_{yq}$ . Here, we introduced a scaled variable  $\eta = \epsilon y_c$  for the translational degree of freedom to highlight separation of length-scales between the translational and internal degrees of freedom of the dumbbell:  $\eta = O(1)$  and  $\epsilon \ll 1$  is the ratio of the average length of the end-to-end vector to the characteristic length-scale of  $y_c$  (e.g., the profile width  $\sigma$ ). The former is  $O(1)$  at sufficiently small shear rates, see Eq. (A18). After these transformations, the Fokker-Planck equation (37) becomes

$$\frac{\partial \bar{P}}{\partial t} = \left[ \frac{\epsilon^2}{2} \frac{\partial^2}{\partial \eta^2} + 2\bar{L}_q + \bar{L}_{yq} \right] \bar{P}. \quad (47)$$

The probability density in terms of the eigenfunctions  $\phi_k(q_i)$  of operators  $b_i^\dagger b_i$  is

$$\bar{P}(\mathbf{q}, \eta, t) = \sum_{k_x, k_y=0}^{\infty} c_{\mathbf{k}}(\eta, t) \phi_{k_x}(q_x) \phi_{k_y}(q_y), \quad (48)$$

where  $\mathbf{k} = (k_x, k_y)$ . The expansion coefficients  $c_{\mathbf{k}}$  are directly related to the moments of the distribution of the end-to-end vector  $\mathbf{q}$ . In particular, it is shown in Appendix C that  $c_{00}$  corresponds to the probability distribution  $n$  of the polymer center of mass and  $c_{11} = n \langle q_x q_y \rangle$ . In what follows, we refer to  $c_{\mathbf{k}}$  as the modes of the end-to-end vector distribution.

Substituting the expansion (48) into Eq. (47), utilizing the relationships (C1), (C3), and (C4), and taking the inner product with  $\phi_{\mathbf{m}}$ , we obtain the following hierarchy of equations:

$$\frac{\partial c_{\mathbf{m}}}{\partial t} = \left[ \frac{\epsilon^2}{2} \frac{\partial^2}{\partial \eta^2} - 2(m_x + m_y) \right] c_{\mathbf{m}} + \hat{L}_{yq, \mathbf{m}}(\{c\}), \quad (49)$$

where  $\mathbf{m} = (m_x, m_y)$  and the operator

$$\begin{aligned} \hat{L}_{yq, \mathbf{m}}(\{c\}) = & \left( \gamma - \epsilon \mathcal{E} \frac{\partial}{\partial \eta} \right) m_x^{1/2} (m_y^{1/2} c_{m_x-1, m_y-1} + (m_y + 1)^{1/2} c_{m_x-1, m_y+1}) \\ & - \epsilon \mathcal{E} \frac{\partial}{\partial \eta} (m_x + 1)^{1/2} (m_y^{1/2} c_{m_x+1, m_y-1} + (m_y + 1)^{1/2} c_{m_x+1, m_y+1}) \end{aligned} \quad (50)$$

describes coupling between dynamics of the end-to-end vector and motion of the center of mass.

Equations (49) are similar to the Brinkman hierarchy for the Kramers equation [19]. The first equation of the hierarchy (49) is

$$\frac{\partial n}{\partial t} = \frac{\epsilon^2}{2} \frac{\partial^2 n}{\partial \eta^2} - \epsilon \mathcal{E} \frac{\partial c_{11}}{\partial \eta} \quad (51)$$

(recall that  $c_{00} = n$ ). This equation indicates that the spatial distribution of the dumbbells is determined by the Brownian diffusive flux (the first term on the right-hand side of Eq.

(51)) and the electrohydrodynamic flux determined by the mode  $c_{11} = n\langle q_x q_y \rangle$  of the end-to-end vector. Evolution of the latter is described by the second equation of the hierarchy (49),

$$\frac{\partial c_{11}}{\partial t} = \left[ \frac{\epsilon^2}{2} \frac{\partial^2}{\partial \eta^2} - 4 \right] c_{11} + \gamma \left( n + \sqrt{2} c_{02} \right) - \epsilon \mathcal{E} \frac{\partial}{\partial \eta} \left[ n + \sqrt{2} (c_{02} + c_{20}) + 2c_{22} \right]. \quad (52)$$

To reduce the infinite hierarchy (49) to a manageable set of equations, first note that all  $c_{\mathbf{m}}$  with  $\mathbf{m} \neq 0$  quickly decay towards their quasi-steady-state values determined by the dumbbell density  $n$ . This fast decay is due to the  $(m_x + m_y)c_{\mathbf{m}}$  terms in Eq. (49); these terms correspond to eigenvalues of the operator  $\bar{L}_{\mathbf{q}}$  describing fluctuations of the end-to-end vector  $\mathbf{q}$ . Eq. (49) indicates that the rate of change of  $c_{\mathbf{m}}$  with  $\mathbf{m} \neq 0$  is  $O(1)$ . On the other hand, Eq. (51) indicates that the rate of change of  $n$  is  $O(\epsilon)$ . Therefore, the non-equilibrium modes  $c_{\mathbf{m}}$  ( $\mathbf{m} \neq 0$ ) relax relatively quickly in response to a slowly changing  $n$ . Hence, we can neglect the time-derivatives in Eq. (49) for  $\mathbf{m} \neq 0$  and perform adiabatic elimination of these fast modes.

The infinite hierarchy (49) can be truncated after its second equation (52) when the local shear rate is small,  $\gamma(y_c) = O(\epsilon)$ , and the electric field is weak or moderate,  $\mathcal{E} \leq O(1)$ . In this case, the leading-order terms of the steady-state version of Eq. (49) yield  $c_{11} = O(\epsilon)n$  and

$$c_{\mathbf{m}} = O(\epsilon^2)n \text{ for } \mathbf{m} \neq (0, 0) \text{ and } \mathbf{m} \neq (1, 1). \quad (53)$$

Rewriting Eq. (52) as

$$c_{11} = \frac{1}{4} \left( \gamma - \epsilon \mathcal{E} \frac{\partial}{\partial \eta} \right) n + O(\epsilon^2)n, \quad (54)$$

we see that, to the leading order, the electrohydrodynamic flux  $c_{11}$  contains contributions of the electrohydrodynamic migration and dispersion represented by the first and second terms on the right-hand side of Eq. (54), respectively. Substituting Eq. (54) into Eq. (51), neglecting the  $O(\epsilon^3)n$  terms, taking the steady-state limit, and returning to the original transverse coordinate  $y_c$ , we recover the mean-field convection-diffusion equation (30) with the transverse velocity and diffusivity given by

$$V_y = \frac{\mathcal{E}\gamma}{4} \quad \text{and} \quad D_{yy}^{\text{eff}} = \frac{1}{2} + \frac{\mathcal{E}^2}{4}. \quad (55)$$

Note that the diffusivity differs from that used in the empirical model (31) which assumed that diffusivity is determined by the local shear. Eq. (55) indicates that  $D_{yy}^{\text{eff}} = D_{yy}^{\text{ss}}(0, \mathcal{E}) =$

$D_{yy}^B + D_{yy}^E(0, \mathcal{E})$ , where  $D_{yy}^B = 1/2$  is the Brownian diffusivity (see Eq. (22)) and  $D_{yy}^E(0, \mathcal{E}) = \mathcal{E}^2/4$  is the electrohydrodynamic dispersion in the absence of shear (see Eq. (28)).

Substituting  $V_y$  and  $D_{yy}^{\text{eff}}$  from Eq. (55) and the local shear  $\gamma(y_c)$  from Eq. (29) into Eq. (33), we conclude that the concentration profile is a Gaussian distribution with the variance

$$\sigma^2 = \frac{D_{yy}^{\text{eff}} H}{\bar{\gamma} \mathcal{E}} = \frac{H}{2\bar{\gamma}} \left( \frac{\mathcal{E}}{2} + \frac{1}{\mathcal{E}} \right). \quad (56)$$

In particular, the optimal field strength corresponding to the minimum profile width is  $\mathcal{E}^* = \sqrt{2}$ . Eq. (56) is consistent with the result of Setaro and Underhill [13] obtained using the method of moments. Moreover, using relationships similar to Eqs. (C6) and (C8) between the modes  $c_m$  and the moments of the end-to-end vector  $\mathbf{q}$ , one can readily verify that steady-state versions of the convection-diffusion equation (51) and the first-moment equation (52) are consistent with equations obtained in [13]. The advantage of the derivation presented in the current work is that it establishes a clear connection between fluctuations of the dumbbell configuration and the electrohydrodynamic dispersion. Furthermore, this approach can be generalized to multi-bead polymer models and more complex electrohydrodynamic models, as well as analysis of developing flows.

Figure 3 compares the profile widths  $\sigma$  predicted by the adiabatic elimination Eq. (56), the empirical mean-field model (31), and results of Brownian dynamics simulations of a dumbbell in a pressure-driven flow. Data for mean shear rates  $\bar{\gamma}$  corresponding Weissenberg numbers  $\overline{\text{Wi}} = \bar{\gamma} \tau_r = 0.5$  and 4 are shown. The dimensionless distance between the channel walls is  $H = 92$ , which corresponds to the channel width in the experiments of Arca *et al.* [3]. For each set of system parameters (electric field strength  $\mathcal{E}$  and mean shear rate  $\bar{\gamma}$ ), at least  $10^4$  trajectories were simulated. As shown in Fig. 3, the predictions of the adiabatic elimination (56) agree with the Brownian dynamics results over a wide range of conditions, beyond the small shear and moderate electric field assumptions made in the derivation of Eq. (56). On the other hand, the empirical mean-field model (31) increasingly deviates from the Brownian dynamics results as  $\mathcal{E}$  and  $\bar{\gamma}$  increase. In addition, Fig. 3 shows asymptotic values of the profile width for  $\mathcal{E} \rightarrow 0$  and  $\mathcal{E} \rightarrow \infty$ , which were obtained from the mean-field model (30) with purely Brownian diffusivity ( $D_{yy}^{\text{eff}} = D_{yy}^B$ ) and purely electrohydrodynamic dispersion ( $D_{yy}^{\text{eff}} = D_{yy}^E(0, \mathcal{E})$ ), respectively. These values agree with the Brownian dynamics results in the corresponding limits thus confirming that Brownian diffusivity and electrohydrodynamic dispersion are dominant at very weak and very strong

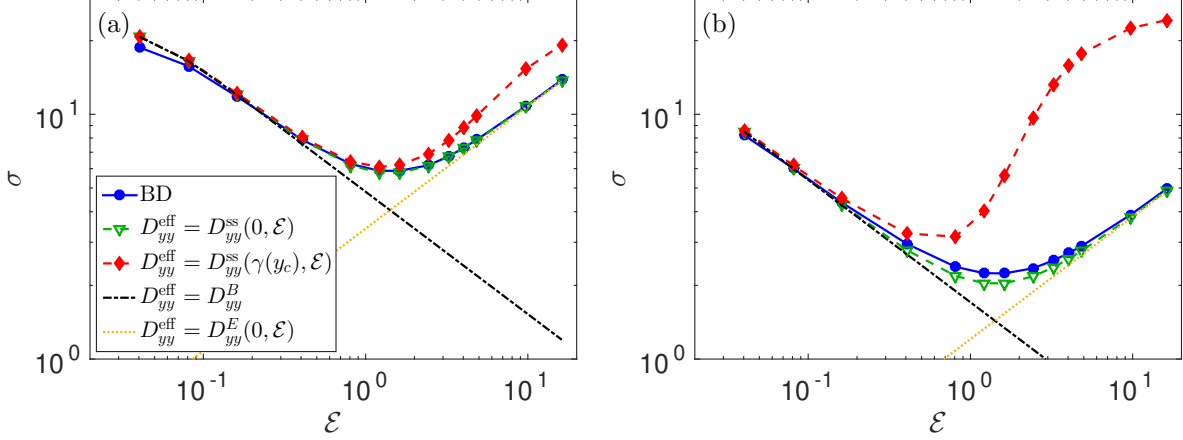


Figure 3: Standard deviations  $\sigma$  of developed concentration profiles in the pressure-driven flows at (a)  $\overline{\text{Wi}} = 0.5$  and (b)  $\overline{\text{Wi}} = 4$ . Results of Brownian dynamics (BD) simulations are compared with the mean-field model (30) with the diffusivity obtained using the adiabatic elimination ( $D_{yy}^{\text{eff}} = D_{yy}^{\text{ss}}(0, \mathcal{E})$ ) and the empirical assumption ( $D_{yy}^{\text{eff}} = D_{yy}^{\text{ss}}(\gamma(y_c), \mathcal{E})$ ). To illustrate contributions of the Brownian diffusivity and the electrohydrodynamic dispersion, predictions of the mean-field models with  $D_{yy}^{\text{eff}} = D_{yy}^B$  and  $D_{yy}^{\text{eff}} = D_{yy}^E(0, \mathcal{E})$  are also shown.

electric fields, respectively.

Simulations of both the harmonic and FENE dumbbell models were performed. These simulations produced nearly identical results for developed profiles, since the transport properties of the harmonic and FENE dumbbells agree for  $\text{Wi} \leq 2$  (see Fig. 2) and the developed concentration profiles are sufficiently narrow to ensure that most of the molecules are located in the region with small local shear rate. Hence, the harmonic approximation remains valid in the high-concentration region even for the largest mean shear rate considered in this work ( $\overline{\text{Wi}} = 4$ ). Therefore, in what follows, we focus on the harmonic dumbbell model.

### C. Discussion

The transverse velocity  $V_y$  of the mean-field model obtained using the adiabatic elimination (Eq. (55)) is consistent with the empirical mean-field assumption (31) that  $V_y$  is determined by local shear  $\gamma(y_c)$ . Namely,  $V_y$  corresponds to the transverse velocity in the simple shear flow which is given by Eq. (28) for the dumbbell model considered here. However, the diffusivity  $D_{yy}^{\text{eff}}$  obtained by the adiabatic elimination is independent of the local

shear rate, which deviates from the empirical mean-field assumption (31) that the effective diffusivity in Eq. (30) should include the shear-dependent dispersion. This discrepancy is explained, in part, by the small- $\gamma$  approximation used in the derivation of Eq. (55), since the  $\gamma$ -dependent term in  $D_{yy}^E$  in the simple shear flow is  $O(\gamma^2)$ , see Eq. (28). However, Fig. 3 shows that the zero-shear value of  $D_{yy}^E$  yields a better agreement with Brownian dynamics simulations than the empirical shear-dependent value (31) even at moderate shear rates.

Despite the quantitative difference between the mean-field models, both qualitatively agree with the experiment and the simulations and predict that  $\sigma(\mathcal{E})$  exhibits a minimum at some optimal  $\mathcal{E} = \mathcal{E}^*$ . The arguments of Section IV A explaining the origin of the optimal electric field for the empirical mean-field model still hold for the adiabatic elimination results, since the key requirements for existence of the optimal field are still satisfied, namely  $V_y \propto \mathcal{E}$  and  $D_{yy}^E \propto \mathcal{E}^2$ .

For weak electric fields, the adiabatic elimination and the empirical mean-field model yield nearly identical results that are in quantitative agreement with the Brownian dynamics simulations. The two mean-field approximations agree at small  $\mathcal{E}$  because, in this case, the contribution of the electrohydrodynamic dispersion  $D_{yy}^E$  to the overall diffusivity is negligible. In fact, completely neglecting  $D_{yy}^E$  and using the approximation  $D_{yy}^{\text{eff}} = D_{yy}^B$  yields essentially the same values of  $\sigma$  at small  $\mathcal{E}$ , as shown in Fig. 3. Since the Brownian diffusivity is independent of local shear (see Eq. (22)), the difference between the adiabatic elimination and the empirical mean-field model vanishes at small  $\mathcal{E}$ .

For strong electric fields, substantial differences exist between the two mean-field approaches, with the adiabatic elimination yielding much better agreement with the Brownian dynamics simulations. Comparison of Fig. 3(a) and (b) reveals that the difference between the mean-field models becomes more significant as the mean shear rate increases. In the simple shear flow, the diffusivity is very sensitive to the shear rate, see Fig. 2 and Eq. (28). Validity of the adiabatic elimination result indicates that electrohydrodynamic dispersion is independent of the local shear rate and corresponds to the dispersion at zero shear rate everywhere in the channel. This in turn suggests lack of time-scale separation between the translational and internal degrees of freedom of the dumbbell, i.e. the polymer does not have time to adjust to changes to its local environment as it traverses the channel at large electric fields.

To confirm this conjecture, we compare time-scales of the dumbbell configuration and

transport in the transverse direction. The former is characterized by the relaxation time  $\tau_r$  of the end-to-end distance and the latter is characterized by the migration and diffusion time-scales  $\tau_V$  and  $\tau_D$  defined as average times that it takes the dumbbell to travel a distance equal to the profile width  $\sigma$ ,

$$\tau_V = \frac{\sigma}{\langle V_y \rangle_y} \quad \text{and} \quad \tau_D = \frac{\sigma^2}{2D_{yy}^{\text{eff}}}. \quad (57)$$

Here,

$$\langle V_y \rangle_y = \int_{-H/2}^{H/2} n(y_c) |V_y(y_c)| dy_c \quad (58)$$

is the transverse migration velocity averaged over the concentration profile  $n(y_c)$  in a fully developed flow. Note that the number density  $n(y_c)$  of dumbbells is normalized so that  $\int_{-H/2}^{H/2} n(y_c) dy_c = 1$ . The values of  $V_y(y_c)$  utilized in Eq. (58) were obtained from the mean-field approximation, i.e. they were taken to correspond the local shear rate  $\gamma(y_c)$ . The definition of  $\tau_D$  uses the diffusivity  $D_{yy}^{\text{eff}} = D_{yy}^{\text{ss}}(0, \mathcal{E})$  at zero shear. This choice is motivated by validity of the adiabatic elimination result, which indicates that the diffusivity of the dumbbell remains equal to  $D_{yy}^{\text{ss}}(0, \mathcal{E})$  throughout the channel. Substituting Eqs. (55), (56), and (58) into Eq. (57), we obtain

$$\frac{\tau_D}{\tau_r} = \frac{H}{2\mathcal{E}\overline{\text{Wi}}} \quad \text{and} \quad \tau_V = \sqrt{2\pi}\tau_D. \quad (59)$$

As expected, the transport time-scales decrease as the electric field strength increases. When  $\mathcal{E} \ll H/\overline{\text{Wi}}$ , the transport time-scales substantially exceed the relaxation time-scale of the internal degrees of freedom of the dumbbell, confirming the key assumption of the empirical mean-field model. In this case, the dumbbell configuration is expected to be determined by the local shear.

However, at strong fields, the transport time-scales are comparable with  $\tau_r$  and the empirical mean-field assumption is invalid. For example, at  $\overline{\text{Wi}} = 4$  and  $\mathcal{E} > 10$ , it takes the dumbbell less time to travel across the entire concentration profile than for its internal fluctuations to relax. Since the transport time-scales are inversely proportional to  $\overline{\text{Wi}}$ , at smaller shear rates the empirical mean-field assumption remains valid for a wider range of  $\mathcal{E}$  as evident from comparison of Fig. 3(a) and (b).

When the transport time-scale is very small, the dumbbell configuration does not adjust to the local environment and is likely to be similar to the configuration near the peak of the

concentration profile, i.e. at zero shear rate. Since the dumbbell configuration in a shearing flow is not affected by the electric field (see Eq. (9)), the zero shear rate configuration is identical to the equilibrium configuration. Hence, the dumbbell degrees of freedom are expected to approach the equilibrium distribution as  $\mathcal{E} \rightarrow \infty$ .

This is confirmed by moments  $M_{km}(y_c) = \langle q_x^k q_y^m \rangle(y_c)$  of the end-to-end vector of the dumbbell. If the empirical mean-field approximation is valid and the dumbbell configuration is determined by local shear, the value of the moment  $M_{km}$  at position  $y_c$  in the pressure-driven flow corresponds to its value in the simple shearing flow at shear  $\gamma = \gamma(y_c)$ . For the harmonic dumbbell approximation, several moments in the simple shear flow are obtained in Appendix A (see Eq. (A18)).

For a pressure-driven flow, the typical effect of  $\mathcal{E}$  on the local dumbbell configuration is demonstrated in Fig. 4, which plots the moment  $M_{11}$  computed for several values of  $\mathcal{E}$  in the fully developed flow at  $\overline{\text{Wi}} = 4$ . For comparison, the moment values corresponding to the local shear,  $M_{11} = \gamma(y_c)/4$ , are also shown. It is evident that at small  $\mathcal{E}$ ,  $M_{11}$  is in good agreement with the empirical mean-field assumption, i.e. the moment in the pressure-driven flow is determined by the local shear. However, as  $\mathcal{E}$  increases, the deviation from the empirical mean-field approximation increases and  $M_{11}(y_c)$  approaches its equilibrium value,  $M_{11} = 0$ , as  $\mathcal{E} \rightarrow \infty$ . Similar trends are observed for other moments  $M_{km}$  and at other mean shear rates (see Fig. S5 and S6 in Supplemental Material [17]).

This confirms that the fast time-scale of the dumbbell transport at large  $\mathcal{E}$  yields a near-equilibrium distribution of the dumbbell end-to-end vector, i.e.  $c_{\mathbf{k}} = 0$  for all  $\mathbf{k} \neq 0$  (see Eq. (48)). In this case, Eq. (52) yields

$$\left( \gamma - \mathcal{E} \frac{d}{dy_c} \right) n = 0. \quad (60)$$

In other words, the electrohydrodynamic convective and dispersion fluxes are balanced and the Brownian diffusion flux is negligible. Therefore,  $n(y)$  is a Gaussian distribution with the variance

$$\sigma_0^2 = \frac{\mathcal{E}H}{4\bar{\gamma}} = \frac{D_{yy}^E(0, \mathcal{E})H}{\bar{\gamma}\mathcal{E}} \quad (61)$$

that corresponds to diffusivity given by the electrohydrodynamic dispersion  $D_{yy}^E(0, \mathcal{E})$  at zero shear. The profile width given by Eq. (61) is in agreement with the adiabatic elimination prediction (56) in the limit of  $\mathcal{E} \rightarrow \infty$  (see also Fig. 3). Hence, the adiabatic elimination result is valid even at strong electric fields, even though its derivation assumed that  $\mathcal{E} \leq O(1)$ .

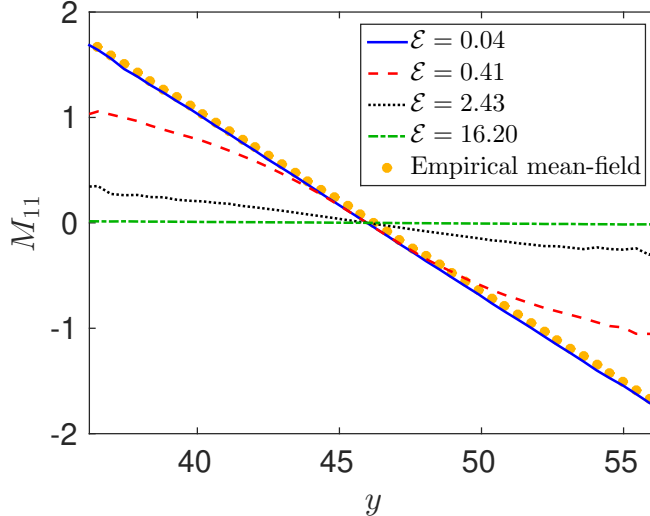


Figure 4: Moment  $M_{11} = \langle q_x q_y \rangle$  of the end-to-end vector  $\mathbf{q}$  obtained from the Brownian dynamics simulations in the pressure-driven flow at  $\overline{\text{Wi}} = 4$  and several  $\mathcal{E}$ . The empirical mean-field approximation to  $M_{11}$ , i.e.  $M_{11}$  determined by the local shear, is shown by circles.

## V. CONCLUSIONS

Diffusive motion of polyelectrolyte molecules with diffuse double layers in a simultaneous shear flow and electric field contains two contributions: Brownian diffusion due to collisions between the polymer and solvent molecules and electrohydrodynamic dispersion caused by fluctuations in the instantaneous electrohydrodynamic velocity of the polymer due to fluctuations in its configuration. At sufficiently strong electric fields, the electrohydrodynamic dispersion dominates the diffusive motion and has a substantial influence on the ability to manipulate polyelectrolyte molecules in microfluidic devices. For example, it introduces a limit on focusing polyelectrolytes on the centerline when using a combination of flow and electric fields.

In the current work we analyzed the electrohydrodynamic dispersion for a dumbbell model of a polyelectrolyte molecule and developed mean-field models connecting dynamics of the internal degrees of freedom with the dumbbell transport. The mean-field model (23), (24) for the dumbbell in a shearing flow provides a direct relationship between fluctuations of the end-to-end vector of the dumbbell and the dispersion. In particular, for ~~a dumbbell in harmonic approximation~~ the harmonic dumbbell, this relationship yields a simple formula

(28) for the dispersion.

For pressure-driven flow in a straight channel, the mean-field model is a convection-diffusion equation (30). For the harmonic ~~approximation to the~~ dumbbell, we obtained the migration and diffusion terms (55) for this equation by performing an adiabatic elimination of the internal degrees of freedom of the dumbbell. The obtained diffusion term contains contributions of both the Brownian diffusivity and the electrohydrodynamic dispersion. It was demonstrated that the latter contributions arise from coupling between the fluctuations of the end-to-end vector of the dumbbell and the translational motion of its center of mass. The developed mean-field model is in agreement with the model obtained by Setaro and Underhill [13] using the kinetic theory. The new derivation presented here establishes a clear connection between the internal degrees of freedom and transport properties of the dumbbell. In addition, we demonstrated that the electrohydrodynamic dispersion is responsible for existence of the optimal electric field for trapping of polyelectrolytes by a combined flow and electric fields.

Although the current work focuses on a relatively simple dumbbell model, the main conclusions are expected to hold for more detailed models of polyelectrolytes. For example, it is shown in Section S1 of Supplemental Material [17] that including hydrodynamic interactions induced by Brownian and conservative forces into the model yields results very similar to those obtained in the absence of these interactions. Another improvement of the model would incorporate a more accurate model for electrohydrodynamic interactions. The short-range electrohydrodynamic model considered in the current work neglects interactions between Kuhn steps of the polyelectrolyte molecule. As shown in [14], this results in a quantitative discrepancy with experimental data, even when simulating a multi-bead polymer model. This necessitates development of a more accurate electrohydrodynamic model. The mean-field relationship Eqs. (23), (24) for the shearing flows is readily applicable to this anticipated future electrohydrodynamic model, since it remains valid as long as Eq. (6) is satisfied.

Furthermore, the qualitative arguments presented in Section IV A show that the mechanism leading to the optimal electric field strength in a pressure-driven flow is applicable for other models for electrohydrodynamic interactions. In addition, the adiabatic elimination for pressure-driven flows presented in Section IV B can be adapted to a different electrohydrodynamic model by making an appropriate change to the operator  $L_{yq}$  describing coupling

between the end-to-end vector and the dumbbell center of mass.

Achieving quantitative agreement with the experiment will require generalizing the current mean-field approach to multi-bead polymer models. **Although the multi-bead model still predicts a non-monotonic dependence of the profile width on the field strength**, comparison between the dumbbell and multi-bead models reveals an important difference between their dispersion terms. Specifically, in the mean-field model (55) for the dumbbell, the dispersion term corresponds to the zero shear rate. On the other hand, in the empirical model (31) proposed and validated for a 20-bead polymer model [14], the dispersion term is determined by local shear. This difference is caused by different time-scales of fluctuations of the electrohydrodynamic velocity. In a multi-bead model, fluctuations of the electrohydrodynamic velocity are dominated by fast fluctuations of individual beads and the contribution of the slow fluctuations of the molecule as a whole are very small [14]. Therefore, in the multi-bead model, the electrohydrodynamic dispersion is less sensitive to local shear and the degrees of freedom relevant to the dispersion respond quickly to changes in the flow environment. These degrees of freedom are absent in a dumbbell, which only captures slow fluctuations of the molecule as a whole.

Therefore, it is expected that a mean-field model for a polymer with a sufficiently large number of beads is similar to the empirical model (31). A systematic study is therefore needed to determine dependence of the electrohydrodynamic dispersion on the number of beads in a polymer model and determine the discretization level necessary for validity of this mean-field model.

## ACKNOWLEDGMENTS

This work was supported by the National Science Foundation (Grant No. 1804302).

## Appendix A: Transverse migration and dispersion of the harmonic dumbbell in a simple shear flow

In this Appendix, we obtain analytical expressions for the electrohydrodynamic migration and dispersion in the transverse direction in the simple shear flow (25) assuming the harmonic ~~approximation of the~~ spring potential (26) and the **leading-order approximation to the** short-

range electrohydrodynamic interactions (27). In this case, the Langevin equation (9) for the end-to-end vector  $\mathbf{q}(t)$  is linear and can be readily solved analytically,

$$q_x(t) = q_x(0)e^{-2t} + \int_0^t e^{-2(t-s)}[\gamma q_y(s) + F_{q,x}^B(s)]ds \quad \text{and} \quad (\text{A1})$$

$$q_y(t) = q_y(0)e^{-2t} + \int_0^t e^{-2(t-s)}F_{q,y}^B(s)ds. \quad (\text{A2})$$

We are interested in solutions at sufficiently large  $t$  so that the influence of the initial conditions (i.e., the first terms on the right hand sides of Eqs. (A1) and (A2)) vanishes. Therefore, in what follows, we assume that  $t \gg 1$ .

The expression (A1) for  $q_x$  contains a contribution of  $q_y$ . It is convenient to express  $q_x$  explicitly in terms of the Brownian force  $\mathbf{F}_q^B$  only. To this end, we substitute Eq. (A2) into Eq. (A1):

$$q_x(t) = \int_0^t e^{-2(t-s)}F_{q,x}^B(s)ds + \gamma \int_0^t \int_0^s e^{-2(t-s')}F_{q,y}^B(s')ds'ds. \quad (\text{A3})$$

The double integral in the second term of Eq. (A3) can be reduced to a single integral by exchanging the order of integration,

$$\begin{aligned} \int_0^t \int_0^s e^{-2(t-s')}F_{q,y}^B(s')ds'ds &= \int_0^t \int_0^t \theta(s-s')e^{-2(t-s')}F_{q,y}^B(s')ds'ds \\ &= \int_0^t e^{-2(t-s')}(t-s')F_{q,y}^B(s')ds', \end{aligned} \quad (\text{A4})$$

where  $\theta(s)$  is the Heaviside step function. Substituting Eq. (A4) into Eq. (A3), we obtain

$$q_x(t) = \int_0^t e^{-2(t-s)} [F_{q,x}^B(s) + \gamma(t-s)F_{q,y}^B(s)] ds. \quad (\text{A5})$$

Substituting Eqs. (A2) and (A5) into Eq. (27), we obtain the following expression for the instantaneous normalized electrohydrodynamic velocity in the transverse direction:

$$\hat{U}_y^E(t) = q_x(t)q_y(t) = \int_0^t ds \int_0^t ds' e^{-2(2t-s-s')} [F_{q,x}^B(s) + \gamma(t-s)F_{q,y}^B(s)] F_{q,y}^B(s'). \quad (\text{A6})$$

Taking into account the fluctuation-dissipation relationship (12), we obtain the following expression for the mean transverse velocity:

$$\langle U_y^E \rangle = \mathcal{E} \langle \hat{U}_y^E \rangle = 4\mathcal{E}\gamma \int_0^t e^{-4(t-s)}(t-s)ds = \frac{\mathcal{E}\gamma}{4}. \quad (\text{A7})$$

The last equality in (A7) was obtained by taking the limit of  $t \rightarrow \infty$ .

To obtain the electrohydrodynamic dispersion, we compute the autocorrelation function of the normalized electrohydrodynamic velocity, see Eqs. (23), (24). It is convenient to rewrite the transverse component of the autocorrelation function (24) as follows:

$$C_{yy}^E(\tau) = \langle \hat{U}_y^E(t) \hat{U}_y^E(t + \tau) \rangle - \langle \hat{U}_y^E \rangle^2. \quad (\text{A8})$$

Without loss of generality, the derivation below assumes that  $\tau \geq 0$ . The first term on the right-hand-side of Eq. (A8) can be written as

$$\langle \hat{U}_y^E(t) \hat{U}_y^E(t + \tau) \rangle = \langle q_x(t) q_y(t) q_x(t + \tau) q_y(t + \tau) \rangle = I_1 + \gamma^2 I_2, \quad (\text{A9})$$

where

$$I_1 = \int_0^t ds_1 \int_0^{t+\tau} ds_2 e^{-2(2t+\tau-s_1-s_2)} \langle F_{q,x}^B(s_1) F_{q,x}^B(s_2) \rangle \langle q_y(t) q_y(t + \tau) \rangle \quad (\text{A10})$$

and

$$I_2 = \int_0^t ds_1 \int_0^{t+\tau} ds_2 e^{-2(2t+\tau-s_1-s_2)} (t - s_1)(t + \tau - s_2) \langle F_{q,y}^B(s_1) F_{q,y}^B(s_2) q_y(t) q_y(t + \tau) \rangle \quad (\text{A11})$$

In writing Eq. (A9) we used the fact that  $q_y$  is independent of  $F_{q,x}^B$  and  $\langle F_{q,x}^B \rangle = 0$ .

It follows from Eqs. (A2) and (12) that

$$\langle q_y(t) q_y(t + \tau) \rangle = \int_0^t ds \int_0^{t+\tau} ds' e^{-2(2t+\tau-s-s')} \langle F_{q,y}^B(s) F_{q,y}^B(s') \rangle = e^{-2\tau} \quad \text{as } t \rightarrow \infty. \quad (\text{A12})$$

Substituting this into Eq. (A10) and applying the fluctuation-dissipation theorem (12), we obtain

$$I_1 = 4e^{-4(t+\tau)} \int_0^t e^{4s} ds = e^{-4\tau} \quad \text{as } t \rightarrow \infty. \quad (\text{A13})$$

Substitute Eq. (A2) into Eq. (A11):

$$I_2 = e^{-4(2t+\tau)} \int_0^t ds_1 \int_0^{t+\tau} ds_2 \int_0^t ds_3 \int_0^{t+\tau} ds_4 e^{2(s_1+s_2+s_3+s_4)} (t - s_1)(t + \tau - s_2) \cdot \langle F_{q,y}^B(s_1) F_{q,y}^B(s_2) F_{q,y}^B(s_3) F_{q,y}^B(s_4) \rangle. \quad (\text{A14})$$

Integrals of type (A14) are computed in Appendix B. Substituting Eq. (B7) into (A14), we

obtain

$$\begin{aligned}
I_2 &= 16e^{-4(2t+\tau)} \left[ \int_0^t ds_1 \int_0^t ds_3 (t-s_1)(t+\tau-s_1)e^{4(s_1+s_3)} \right. \\
&\quad + \int_0^t ds_1 \int_0^{t+\tau} ds_2 (t-s_1)(t+\tau-s_2)e^{4(s_1+s_2)} \\
&\quad \left. + \int_0^t ds_1 \int_0^t ds_2 (t-s_1)(t+\tau-s_2)e^{4(s_1+s_2)} \right] \\
&= \frac{e^{-4\tau}(3+8\tau)}{16} + \frac{1}{16} \quad \text{as } t \rightarrow \infty.
\end{aligned} \tag{A15}$$

Substituting Eqs. (A13) and (A15) into Eq. (A9) and then substituting the result together with Eq. (A7) into Eq. (A8), we obtain

$$C_{yy}^E(\tau) = \langle \hat{U}_y^E(t) \hat{U}_y^E(t+\tau) \rangle - \frac{\gamma^2}{16} = \left( 1 + \frac{\gamma^2(3+8\tau)}{16} \right) e^{-4\tau}. \tag{A16}$$

Thus, the electrohydrodynamic dispersion of the harmonic dumbbell is

$$D_{yy}^E = \mathcal{E}^2 \int_0^{+\infty} C_{yy}^E(\tau) d\tau = \frac{\mathcal{E}^2}{4} \left( 1 + \frac{5\gamma^2}{16} \right). \tag{A17}$$

The first equality in Eq. (A17) follows from Eq. (23) because diagonal components of the matrix  $\mathbf{C}^{\mathbf{E}}(\tau)$  are symmetric with respect to time,  $C_{ii}^E(\tau) = C_{ii}^E(-\tau)$ .

In conclusion of this Appendix, we compute several moments of the end-to-end vector  $\mathbf{q}$  which are utilized in verification of the mean-field assumption for the pressure-driven flow (see Fig. 4, S5, and S6):

$$\langle q_x q_y \rangle = \frac{\gamma}{4}, \quad \langle q_x^2 \rangle = 1 + \frac{\gamma^2}{8}, \quad \langle q_y^2 \rangle = 1, \quad \langle q_x^2 q_y^2 \rangle = 1 + \frac{\gamma^2}{4}. \tag{A18}$$

## Appendix B: Calculation of integral (A14)

The purpose of this Appendix is to compute the integral

$$I = \int_0^{t_1} ds_1 \int_0^{t_2} ds_2 \int_0^{t_3} ds_3 \int_0^{t_4} ds_4 f(s_1, s_2, s_3, s_4) \langle \Gamma(s_1) \Gamma(s_2) \Gamma(s_3) \Gamma(s_4) \rangle, \tag{B1}$$

where  $\Gamma(s)$  is a random process with Gaussian distribution, zero mean, and the autocorrelation function  $\langle \Gamma(s) \Gamma(s+\tau) \rangle = 4\delta(\tau)$ . The challenge in computing this integral is handling the 4-variable correlation when even the 2-variable correlation is singular (a  $\delta$ -function). To do this, we introduce a Wiener process  $W(s)$  corresponding to the Brownian force  $\Gamma(s)$ ,

$$dW(s) = \Gamma(s) ds, \tag{B2}$$

and rewrite Eq. (B1) as a limit of the Riemann sum, i.e.

$$\begin{aligned}
I &= \left\langle \int_0^{t_1} dW(s_1) \int_0^{t_2} dW(s_2) \int_0^{t_3} dW(s_3) \int_0^{t_4} dW(s_4) f(s_1, s_2, s_3, s_4) \right\rangle \\
&= \lim_{\Delta t \rightarrow 0} \sum_{i_1=0}^{N_1} \sum_{i_2=0}^{N_2} \sum_{i_3=0}^{N_3} \sum_{i_4=0}^{N_4} f(s_1, s_2, s_3, s_4) \langle \Delta W_{i_1} \Delta W_{i_2} \Delta W_{i_3} \Delta W_{i_4} \rangle, \tag{B3}
\end{aligned}$$

where  $N_j = [t_j/\Delta t]$ ,  $s_j = i_j \Delta t$  ( $j = 1, \dots, 4$ ), and

$$\Delta W_i = \int_{i\Delta t}^{(i+1)\Delta t} \Gamma(s) ds \tag{B4}$$

is a Gaussian variable with zero mean and autocorrelation

$$\langle \Delta W_i \Delta W_j \rangle = 4\delta_{ij} \Delta t. \tag{B5}$$

Therefore,

$$\langle \Delta W_{i_1} \Delta W_{i_2} \Delta W_{i_3} \Delta W_{i_4} \rangle = 16\Delta t^2 (\delta_{i_1 i_2} \delta_{i_3 i_4} + \delta_{i_1 i_3} \delta_{i_2 i_4} + \delta_{i_1 i_4} \delta_{i_2 i_3} + 3\delta_{i_1 i_2} \delta_{i_1 i_3} \delta_{i_1 i_4}). \tag{B6}$$

The last term in Eq. (B6) corresponds to the 4-th moment of the Gaussian variable  $\Delta W_i$ .

Substituting Eq. (B6) into Eq. (B3), we obtain

$$\begin{aligned}
I &= 16 \lim_{\Delta t \rightarrow 0} \Delta t^2 \left[ \sum_{i_1=0}^{N_1 \wedge N_2} \sum_{i_3=0}^{N_3 \wedge N_4} f(s_1, s_1, s_3, s_3) + \sum_{i_1=0}^{N_1 \wedge N_3} \sum_{i_2=0}^{N_2 \wedge N_4} f(s_1, s_2, s_1, s_2) \right. \\
&\quad \left. + \sum_{i_1=0}^{N_1 \wedge N_4} \sum_{i_2=0}^{N_2 \wedge N_3} f(s_1, s_2, s_2, s_1) + \sum_{i_1=0}^{N_1 \wedge N_2 \wedge N_3 \wedge N_4} f(s_1, s_1, s_1, s_1) \right] \\
&= 16 \left[ \int_0^{t_1 \wedge t_2} ds_1 \int_0^{t_3 \wedge t_4} ds_3 f(s_1, s_1, s_3, s_3) + \int_0^{t_1 \wedge t_3} ds_1 \int_0^{t_2 \wedge t_4} ds_2 f(s_1, s_2, s_1, s_2) \right. \\
&\quad \left. + \int_0^{t_1 \wedge t_4} ds_1 \int_0^{t_2 \wedge t_3} ds_2 f(s_1, s_2, s_2, s_1) \right]. \tag{B7}
\end{aligned}$$

Here,  $x \wedge y = \min(x, y)$ .

### Appendix C: Details of analysis of the Fokker-Planck equation for the harmonic dumbbell

In this section we summarize properties of eigenfunctions  $\phi_k$  of the operators  $b_i^\dagger b_i$  ( $i = x, y$ ) that describe the probability density of the end-to-end vector of the harmonic dumbbell.

Here,  $b_i^\dagger$  and  $b_i$  are the boson creation and annihilation operators defined in Eq. (43). Further information on properties of these operators is available, e.g., in [19].

The eigenvalues of the operator  $b_i^\dagger b_i$  are non-negative integers,

$$b_i^\dagger b_i \phi_k(q_i) = k \phi_k(q_i), \quad i = x, y, \quad k = 0, 1, 2, \dots \quad (\text{C1})$$

The eigenfunction corresponding to zero eigenvalue is

$$\phi_0(q_i) = C_0 e^{-q_i^2/4}, \quad (\text{C2})$$

where the normalization constant  $C_0 = (2\pi)^{-1/4}$  is chosen so that  $\|\phi_0\| = 1$ .

Application of the operators  $b_i$  and  $b_i^\dagger$  to the eigenfunction  $\phi_k$  of the operator  $b_i^\dagger b_i$  transforms  $\phi_k$  into eigenfunctions  $\phi_{k-1}$  and  $\phi_{k+1}$ , respectively,

$$b_i \phi_k(q_i) = k^{1/2} \phi_{k-1}(q_i), \quad (\text{C3})$$

$$b_i^\dagger \phi_k(q_i) = (k+1)^{1/2} \phi_{k+1}(q_i). \quad (\text{C4})$$

The  $k^{1/2}$  and  $(k+1)^{1/2}$  factors in these equations ensure that  $\|\phi_k\| = 1$  for all  $k$ . Since the operator  $b_i^\dagger b_i$  is self-adjoint, its eigenfunctions  $\phi_k$  form an orthonormal set.

The coefficients  $c_{\mathbf{k}}$  of the eigenfunction expansion (48) are directly related to the number density of the dumbbell center of mass and moments of its end-to-end vector. It follows from Eqs. (40) and (C2) that

$$P(\mathbf{q}, y_c, t) = \bar{P}(\mathbf{q}, y_c, t) \phi_0(q_x) \phi_0(q_y). \quad (\text{C5})$$

Then the number density of the dumbbell is

$$n(y_c, t) = \int P(\mathbf{q}, y_c, t) d\mathbf{q} = \int \bar{P}(\mathbf{q}, y_c, t) \phi_0(q_x) \phi_0(q_y) d\mathbf{q} = c_{00}(y_c, t). \quad (\text{C6})$$

Here, we used the expansion (48) and the fact that the eigenfunctions  $\phi_k$  are orthonormal.

To obtain the moment  $\langle q_x q_y \rangle(y_c, t)$  of the end-to-end vector, we note that

$$\phi_1(q_i) = b_i^\dagger \phi_0 = C_0 q_i e^{-q_i^2/4} = q_i \phi_0(q_i). \quad (\text{C7})$$

Therefore,

$$n \langle q_x q_y \rangle = \int P(\mathbf{q}, y_c, t) q_x q_y d\mathbf{q} = \int \bar{P}(\mathbf{q}, y_c, t) \phi_1(q_x) \phi_1(q_y) d\mathbf{q} = c_{11}(y_c, t). \quad (\text{C8})$$

Similar approach can be used to obtain relationships between other coefficients  $c_{\mathbf{k}}$  and moments of the end-to-end vector.

- 
- [1] J. Zheng and E. S. Yeung, Anomalous radial migration of single DNA molecules in capillary electrophoresis, *Anal. Chem.* **74**, 4536 (2002).
  - [2] J. Zheng and E. S. Yeung, Mechanism for the separation of large molecules based on radial migration in capillary electrophoresis, *Anal. Chem.* **75**, 3675 (2003).
  - [3] M. Arca, J. E. Butler, and A. J. C. Ladd, Transverse migration of polyelectrolytes in microfluidic channels induced by combined shear and electric fields, *Soft Matter* **11**, 4375 (2015).
  - [4] M. Arca, A. J. C. Ladd, and J. E. Butler, Electro-hydrodynamic concentration of genomic length DNA, *Soft Matter* **12**, 6975 (2016).
  - [5] R. J. Montes, J. E. Butler, and A. J. C. Ladd, Trapping DNA with a high throughput microfluidic device, *Electrophoresis* **40**, 437 (2019).
  - [6] B. E. Valley, A. D. Crowell, J. E. Butler, and A. J. C. Ladd, Electro-hydrodynamic extraction of DNA from mixtures of DNA and bovine serum albumin, *Analyst* **145**, 5532 (2020).
  - [7] O. B. Usta, J. E. Butler, and A. J. C. Ladd, Transverse migration of a confined polymer driven by an external force, *Phys. Rev. Lett.* **98**, 098301 (2007).
  - [8] J. E. Butler, O. B. Usta, R. Kekre, and A. J. C. Ladd, Kinetic theory of a confined polymer driven by an external force and pressure-driven flow, *Phys. Fluids* **19**, 113101 (2007).
  - [9] R. Kekre, J. E. Butler, and A. J. C. Ladd, Role of hydrodynamic interactions in the migration of polyelectrolytes driven by a pressure gradient and an electric field, *Phys. Rev. E* **82**, 050803(R) (2010).
  - [10] W.-C. Liao, N. Watari, S. Wang, X. Hu, R. G. Larson, and L. J. Lee, Conformation dependence of DNA electrophoretic mobility in a converging channel, *Electrophoresis* **31**, 2813 (2010).
  - [11] H. Pandey and P. T. Underhill, Coarse-grained model of conformation-dependent electrophoretic mobility and its influence on DNA dynamics, *Phys. Rev. E* **92**, 052301 (2015).
  - [12] A. J. C. Ladd, Electrophoresis of sheared polyelectrolytes, *Mol. Phys.* **116**, 3121 (2018).
  - [13] A. C. Setaro and P. T. Underhill, Dumbbell kinetic theory for polymers in a combination of flow and external electric field, *Phys. Rev. E* **100**, 052501 (2019).
  - [14] D. I. Kopelevich, S. He, R. J. Montes, and J. E. Butler, Mesoscopic models for electro-

- hydrodynamic interactions of polyelectrolytes, *J. Fluid Mech.* **915**, A59 (2021).
- [15] R. M. Jendrejack, J. J. De Pablo, and M. D. Graham, Stochastic simulations of DNA in flow: Dynamics and the effects of hydrodynamic interactions, *J. Chem. Phys.* **116**, 7752 (2002).
- [16] M. Doi and S. F. Edwards, *The Theory of Polymer Dynamics* (Oxford University Press, 1986).
- [17] See Supplemental Material for (1) analysis of a dumbbell with hydrodynamic interactions, (2) comparison of configurations of the harmonic and FENE dumbbells in a shearing flow, and (3) additional plots of moments of the end-to-end vector in the pressure-driven flow.
- [18] H. R. Warner, Kinetic theory and rheology of dilute suspensions of finitely extendible dumbbells, *Ind. Eng. Chem. Fundam.* **11**, 379 (1972).
- [19] H. Risken, *The Fokker-Planck Equation. Methods of Solution and Applications* (Springer-Verlag, Berlin, 1984).
- [20] J. Rotne and S. Prager, Variational treatment of hydrodynamic interaction in polymers, *J. Chem. Phys.* **50**, 4831 (1969).
- [21] R. Kekre, J. E. Butler, and A. J. C. Ladd, Comparison of Boltzmann and Brownian Dynamics simulations of polymer migration in confined flows, *Phys. Rev. E* **82**, 011802 (2010).